Computational Studies Of Flow Field And Associated Aerodynamic Characteristics Of Wing-Body Configurations

Satyaprakash[1] , S. Senthilkumar[2], S. Dashlin Jeno[3]

[1]Sc/Engr 'F', Aerodynamics & Performance Directorate (ARD&P), Aeronautical Development Agency (ADA), Bangalore
[2]Department of Aeronautical Engineering, Anna University, Chennai
[3]Nehru Institute of Engineering and Technology, Coimbatore

ABSTRACT

A Computational study is conducted to investigate flow field around a Wing-Body configuration. A Wing-Body model is created using CATIA V5 and Structured Grids were generated by ANSYS ICEM CFD. Numerical Analysis is done using ANSYS FLUENT solver. Different Grids are tested for Grid Independence Test to conclude that the solution is independent of further mesh refinements. Flow field was initialized with free-stream values. Calculations were done with the three turbulence models such as Spalart –Allmaras model, Realizable $k-\epsilon$ model and Stress Transport (SST) $k-\omega$ model. The three turbulence models were compared with experimental results. The prediction shows that CFD results provide acceptable agreement to experimental observations. Convergence was monitored in terms of Lift, Drag and Moment. Pressure distribution has been studied over the surface of the entire model. Chord wise Cp variation computed is compared with experimental data for 8 sections along the wing span. Adequacy of grid resolution was checked in terms of y+. The resulting y+ values were observed to be less than 1 at all the near body grid points. The surface streamline pattern for wing and different cross section are plotted to study the flow separation at wing-body junction.

NOMENCLATURE

ρ	Fluid Density
p	Thermodynamic Pressure
E	Total Energy
H	Total Enthalpy Per Unit Mass
u, v, w	Cartesian components of the velocity vector**u**
μ	Coefficient of Molecular Viscosity
T	Temperature
k	Coefficient of Thermal Conductivity
R	Gas Constant
Pr_t	Turbulent Prandtl Number
μ_t	Turbulence Viscosity
ν	Molecular Viscosity
M	Mach number
α	Angle of attack
Re	Reynolds Number

1. INTRODUCTION

In 1980's, the researchers believed that "Computational Fluid Dynamics is capable of simulating flow in complex geometries with simple physics or flow with simple geometries with more complex physics". But this is not true anymore, due to the development in computers and algorithms. CFD is widely accepted as a key tool for aerodynamic design. Reynolds Average Navier-Stokes (RANS) solutions are a common tool, and methodologies like Large Eddy Simulation (LES) that were once confined to simple canonical flows, are moving to complex engineering applications. Many comparative studies have been carried out for different models to understand the capabilities of numerical solution over experimental solution. In this study, a Wing-Body model is studied and detailed comparisons are made between the computed and experimental results.

2. GOVERNING EQUATIONS

Fluent solves the governing equations of conservation of mass, momentum and energy for the flow of viscous, compressible and conducting fluids. For an arbitrary control volume V with differential surface area dS, the equations, in integral form, are written as

$$\frac{\partial}{\partial t}\int_V \mathbf{U}dV + \oint_S \mathbf{F}^{inv}.\mathbf{dS} = \oint_S \mathbf{F}^{v}.\mathbf{dS}$$

IJERT

Where

$$\mathbf{U} = \begin{bmatrix} \rho \\ \rho u \\ \rho v \\ \rho w \\ \rho \mathrm{E} \end{bmatrix}$$

is the vector of conserved variables and

$$\mathbf{F}^{inv}(\mathbf{U}) = \begin{bmatrix} \rho \mathbf{u} \\ \rho \mathbf{u} u + p \mathbf{i}_x \\ \rho \mathbf{u} v + p \mathbf{i}_y \\ \rho \mathbf{u} w + p \mathbf{i}_z \\ \rho \mathbf{u} H \end{bmatrix}$$

$$\mathbf{F}^{v}(\mathbf{U}) = \begin{bmatrix} 0 \\ \tau_{xx}\mathbf{i}_x + \tau_{xy}\mathbf{i}_y + \tau_{xz}\mathbf{i}_z \\ \tau_{yx}\mathbf{i}_x + \tau_{yy}\mathbf{i}_y + \tau_{yz}\mathbf{i}_z \\ \tau_{zx}\mathbf{i}_x + \tau_{zx}\mathbf{i}_y + \tau_{zz}\mathbf{i}_z \\ \Pi_x \mathbf{i}_x + \Pi_y \mathbf{i}_y + \Pi_z \mathbf{i}_z \end{bmatrix}$$

are the inviscid and viscous flux vectors, respectively. The terms in energy flux are written as

$$\Pi_x = (\tau . \mathbf{u})_x - q_x$$

$$\Pi_y = (\tau . \mathbf{u})_y - q_y$$
$$\Pi_z = (\tau . \mathbf{u})_z - q_z$$

In these equations, ρ represents the fluid density, p is thermodynamic pressure, E is the total energy and H is the total enthalpy per unit mass and u, v, w are the Cartesian components of the velocity vector **u.**

The viscous effects are represented by the shear stress tensor $(\tau_{xx}, \tau_{xy}, \tau_{xz}, \tau_{yx},\ \tau_{yy}, \tau_{yz}, \tau_{zx}, \tau_{zy}, \tau_{zz})$ and the heat conduction vector q $(= q_x i_x + q_y i_y + q_z i_z$. Here i_x, i_y, i_z are the basis vectors in x, y, z directions, respectively.

The fluid is assumed to be Newtonian. It is also assumed to satisfy Stokes' hypothesis. With these assumptions, the components of the Shear Stress tensor may be written as

$$\tau_{xx} = 2\mu \frac{\partial u}{\partial x} - \frac{2}{3}\mu \left(\frac{\partial u}{\partial x} + \frac{\partial v}{\partial y} + \frac{\partial w}{\partial z} \right)$$

$$\tau_{yy} = 2\mu \frac{\partial v}{\partial y} - \frac{2}{3}\mu \left(\frac{\partial u}{\partial x} + \frac{\partial v}{\partial y} + \frac{\partial w}{\partial z} \right)$$

$$\tau_{zz} = 2\mu \frac{\partial w}{\partial z} - \frac{2}{3}\mu \left(\frac{\partial u}{\partial x} + \frac{\partial v}{\partial y} + \frac{\partial w}{\partial z} \right)$$

$$\tau_{xy} = \mu \left(\frac{\partial u}{\partial y} + \frac{\partial v}{\partial x} \right)$$

$$\tau_{xz} = \mu \left(\frac{\partial u}{\partial z} + \frac{\partial w}{\partial x} \right)$$

$$\tau_{yz} = \mu \left(\frac{\partial v}{\partial z} + \frac{\partial w}{\partial y} \right)$$

where μ is the coefficient of molecular viscosity.

The heat flux vector for a Newtonian fluid follow the Fourier's law. The components heat conduction flux are expressed as

$$q_x = -k \frac{\partial T}{\partial x},\quad q_y = -k \frac{\partial T}{\partial y},\quad q_z = -k \frac{\partial T}{\partial z}$$

where T is the temperature and k is the coefficient of thermal conductivity.

If the fluid is assumed to be thermally perfect ideal gas and the closure is provided by the equation of state

$$p = \rho R T$$

linking the thermodynamic variables ρ, T and p. T is temperature and R is gas constant.

Assuming further that the gas is calorically perfect, then the internal and total energy are given by

$$E = e + \frac{u^2 + v^2 + w^2}{2}$$

and $$H = E + \frac{P}{\rho}$$

where $e = C_v T$, $C_p - C_v = R$, and $\gamma = \frac{C_p}{C_v}$.

It is convenient to express the pressure in terms of conservative variables. Using the relations between total enthalpy, total energy and combining with the above definition of equation of state, we finally obtain the following expression relating pressure with the conservative variables

$$p = \rho(\gamma - 1)\left(E - \frac{u^2 + v^2 + w^2}{2} \right)$$

The coefficient of molecular viscosity μ for a perfect gas is dependent on temperature. The dependent of pressure is however weak.

The molecular viscosity can be obtained by Sutherland law given by

IJERT

$$\mu = 1.45\text{x}10^{-6}\,\frac{T^{3/2}}{T+110}\ \text{Kg/m3}$$

In the above expression, T is temperature of air in Kelvin (K).

For turbulent flows, $\mu$and $k$are replaced by $\mu + \mu_t$and $k + k_t$ respectively, where $\mu_t$is turbulence viscosity which is calculated using a turbulence model and k_t is obtained from $k_t = \frac{\mu t}{Prt}$. The turbulent Prandtl number,Pr_t for air flows is taken to be 0.9.

3. GEOMETRY

The basic planform characteristics of the model are depicted in Figure 1, including the position of the wing. The length of the model is 1192mm, span of the wing is 1171.29mm and the semi-span of the wing is 585.645mm. The model is developed using CATIA V5. The half model of the aircraft is utilized for CFD simulation, because the configuration was symmetric, and this procedure could save file size and use less element number. This has the great advantage of faster and more economic processing time of CFD calculation as against CFD simulation employed for the whole aircraft model. Figure 2 shows the Wing-Body Aircraft model.

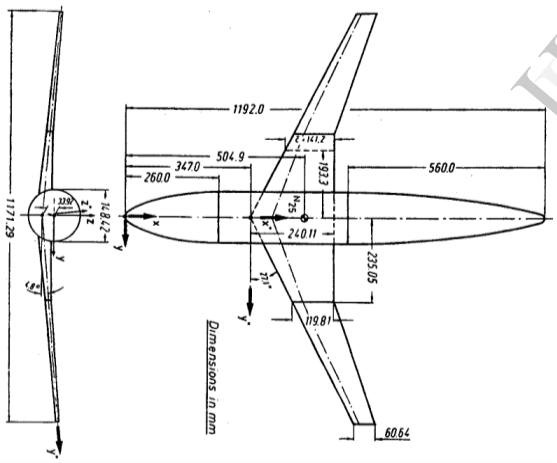

Fig 1. Wing-Body Planform

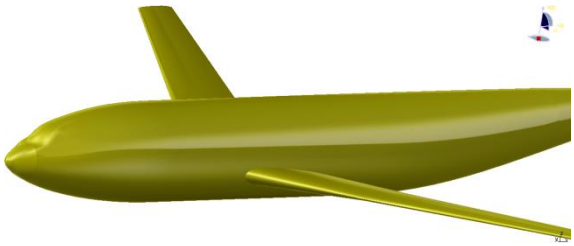

Fig 2. Wing-Body CATIA Model

4. GRID GENERATION

Quadrilateral and hexahedral elements have been proved to be useful for finite element and finite volume methods, and for some applications triangles or tetrahedral are preferred. Structured Grid is generated by using ANSYS ICEM CFD. ANSYS FLUENT operates on unstructured hybrid grids. Thus, structured grids are converted to unstructured grids and all the calculations in present study were done on grids with hexahedral elements. The grids were refined near the body surfaces to resolve the boundary layers. The initial height of hexahedral is 0.001mm to capture the shear effects. The size of coarse is ~7 million and fine grid is ~12million.

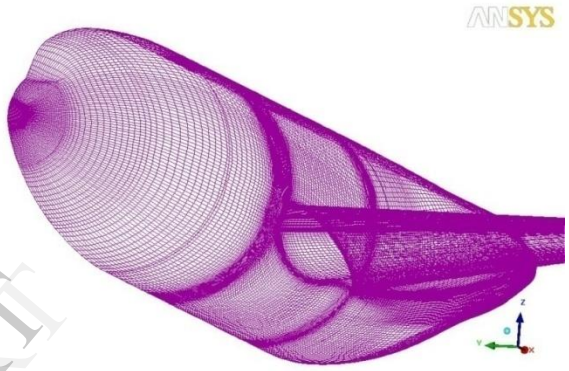

Fig 3.Surface grid of Wing-Body Configuration

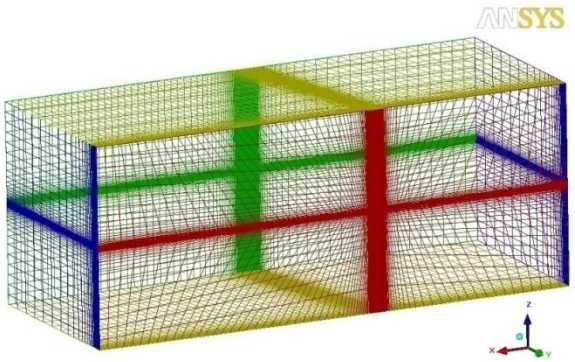

Fig 4.Computational Domain Grid by using Multi Block type

5. Boundary conditions

Table 1 shows the flow conditions of the Wing-Body model. Figure 5 shows Boundary conditions applied in computational domain.

IJERT

M	0.75
Re (based on mean chord, L=0.1412m)	$3x10^6$
T_∞	288.15 K
P_∞	123200.98 N/m^2
α	1.232^o

Table 1. Flow conditions

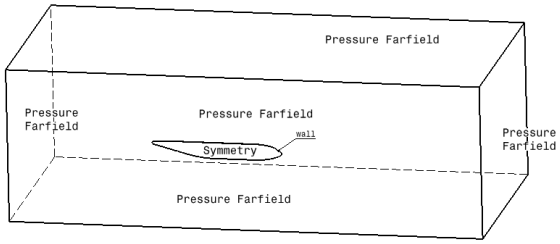

Fig 5. Computational Domain with Boundary Conditions

6. RESULTS AND DISCUSSION

6.1 Grid Independence Tests

A general method for determining the most appropriate mesh configuration is a grid independence test, where different meshes are tested until the solution is independent of further mesh refinements, by matching the numerical results to bench mark tests and/or experimental data. This in itself is a time-consuming process. Grid independence tests are performed to investigate the influence of grid refinement on the solution and corresponding results are presented here for two of the computational grids used. For this purpose, Spalart-Allmaras turbulence model is used and the results are shown in figure 6 and table 2.

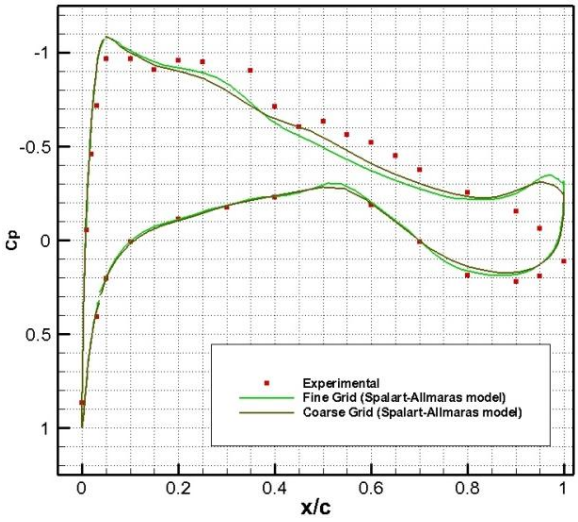

Fig 6.Grid convergence usingCpvs x/c at 0.150 of wing span section

Methods		α	C_L
Experimental		1.230	0.5979
Numerical Solution	Coarse grid	1.230	0.36
	Fine grid	1.230	0.6

Table 2.Grid convergence using CL vsα at 0.150 of wing span section

6.2 Convergence Graphs

The convergence was monitored using the scaled residuals of the Lift coefficient and Drag coefficient. For different turbulence model, calculations were computed for 15000 iterations. The solution was converged when the residuals of the conserved variables no longer varied. The convergence history of coefficient of lift is shown in Figure 7 for different turbulence models.

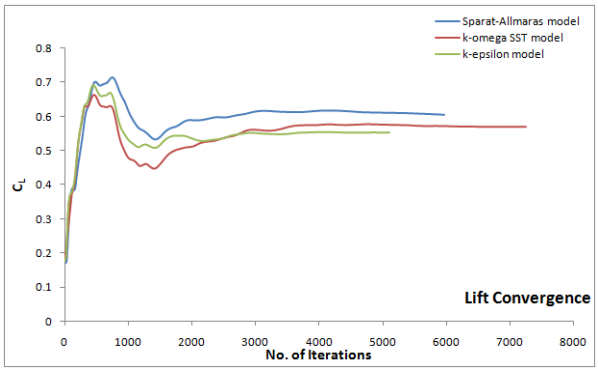

Fig 7.Lift Coefficient versus Number of Iterations for different turbulence model

IJERT

6.3 Wall Y+ Approach

Turbulence flows are significantly affected by the presence of walls due to the no-slip condition resulting in large gradients in the solution variables in this viscosity affected region. **y+< 5** is in the viscous sublayer, **5 < y+< 30** is in buffer region, **30 < y+< 300**, which is fully turbulent portion.

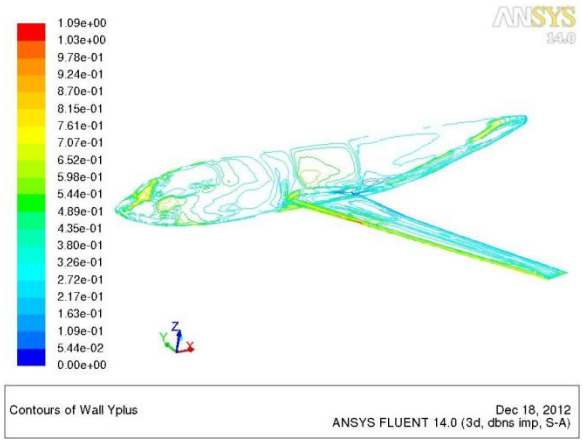

Fig 8.Grid resolution (Near wall Y+) contours at M=0.75, α=1.230

Figure 8 shows near wall Y+ contour of Wing-Body configuration. The Y+ values for the fine grid configuration is 1.09 corresponding to resolution in the viscous sublayer(y+<5), indicates adequate grid resolution.

6.4 Pressure Distribution

Pressure contour of Wing-Body configuration is shown in figure 9 at Mach Number 0.75 and Alpha 0.232 using Tecplot 360.

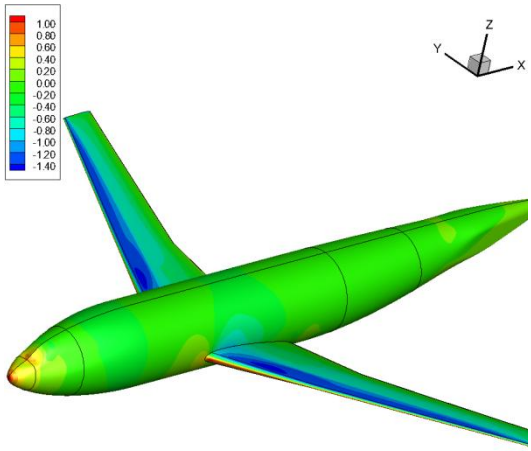

Fig 9.Pressure Contour at M=0.75, α=1.230 using Tecplot 360 (Spalart-Allmaras)

6.5 Pressure Coefficient vs Chord Ratio

Pressure coefficient variation with respect to chord ratio is calculated for various cross-sections and compared with wind tunnel data. Experimental Results were compared with different turbulence models for 8 wing cross-sections and is shown in figure 10(a-h). Turbulence models include Spalart – Allmaras, Realizable $k-\epsilon$ and Stress Transport (SST) $k-\omega$ Turbulence model.

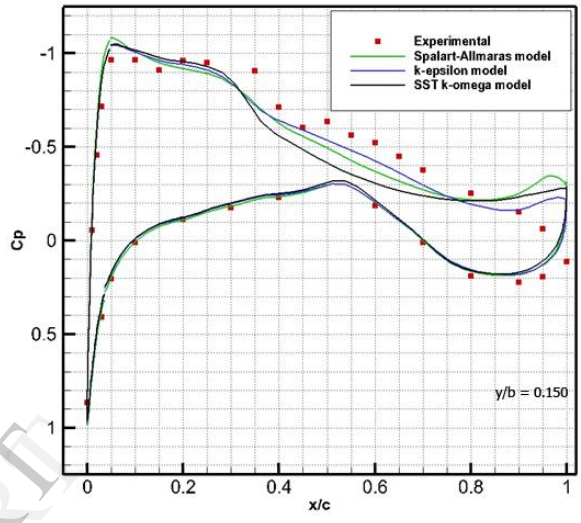

Fig 10(a). Wing span section, y/b=0.150

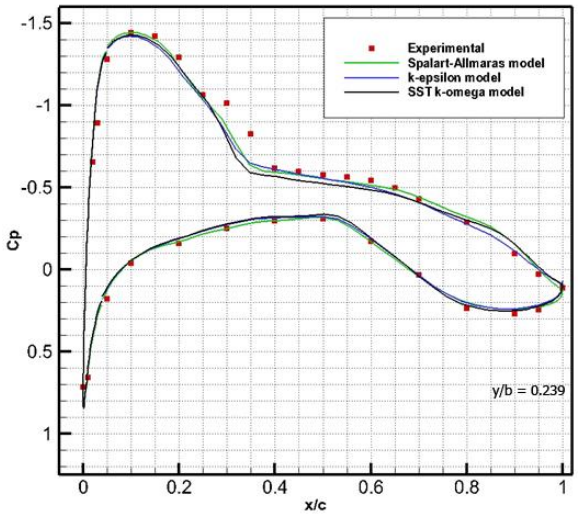

Fig 10(b). Wing span section, y/b=0.239

IJERT

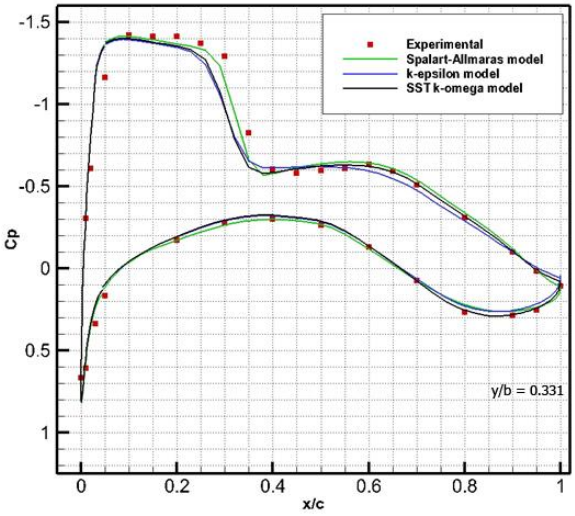

Fig 10(c). Wing span section, y/b=0.331

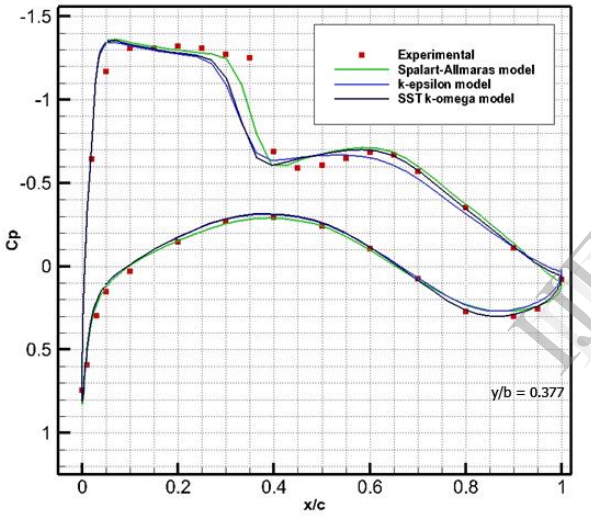

Fig 10(d). Wing span section, y/b=0.377

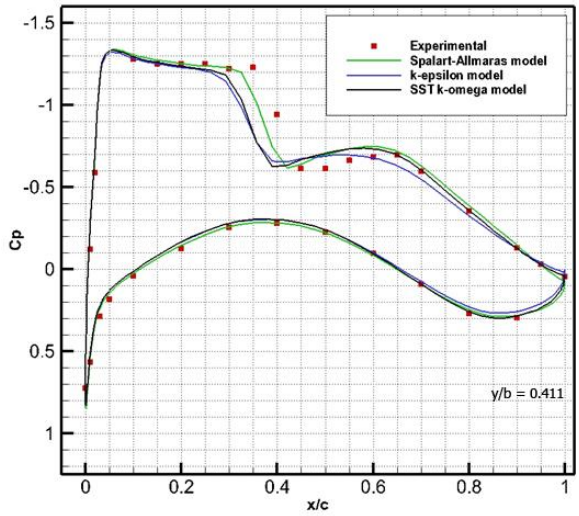

Fig 10(e). Wing span section, y/b=0.411

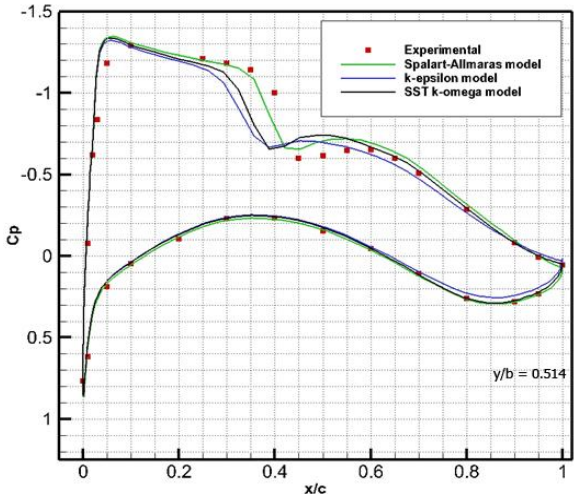

Fig 10(f). Wing span section, y/b=0.514

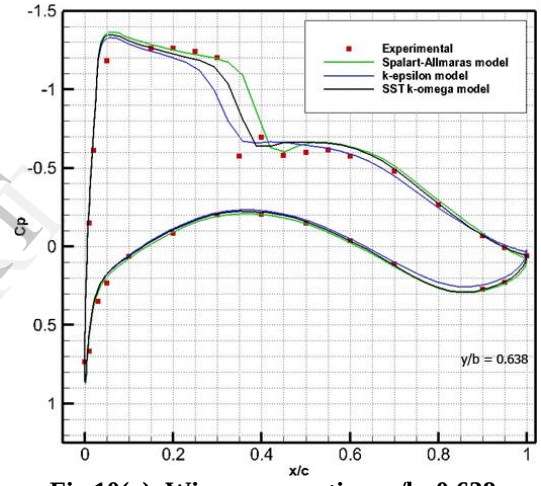

Fig 10(g). Wing span section, y/b=0.638

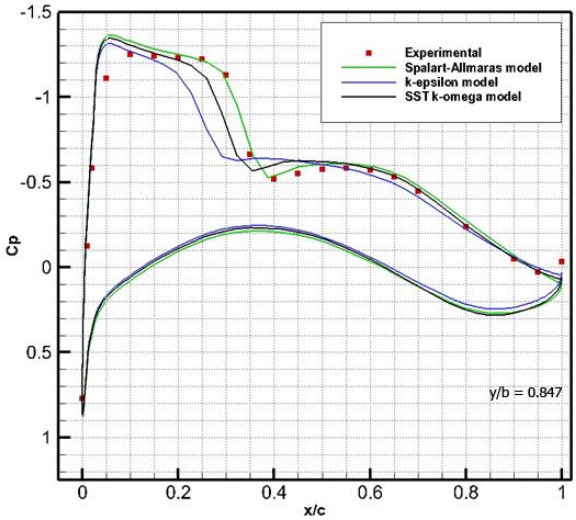

Fig 10(h). Wing span section, y/b=0.847

Fig 10(a-h).Comparison of computed Cp with experimental data for different wing span sections

IJERT

The computed Cp shows that three turbulence models gives reasonable good agreement with the experimental data. The results are plotted using Tecplot 360.

6.6 Lift Coefficient vs Alpha

Lift coefficient versus Angle of Attack (α) is compared between Experimental and numerical results. Table 3 shows the comparison of C_L vs. α for different turbulence models. Spalart-Allmaras models, shows good match with experimental value, when compared to others.

Methods		α	C_L
Experimental		1.230	0.5979
Numerical Solution Turbulence Model	Spalart-Allmaras	1.230	0.6
	k-epsilon	1.230	0.568
	k-omega SST model	1.230	0.554

Table 3. Comparing CL versus α with different turbulence model

6.7 Flow Separation

Flow separation study has been carried out for the model. Flow separations are visualised at Fuselage-wing junction at low Angle of Attack (α=1.230). Fig 11(a-b) shows streamline pattern of the model. Fig 12(a-c) shows the streamline pattern of different turbulent model at0.150 of wing span section. Flow separation are clearly captured in Spalart-Allmaras and SST $k-\omega$, when comparing Realizable $k-\epsilon$ model. Results shows that flow separation can be minimized by providing fairing at Fuselage-wing junction.

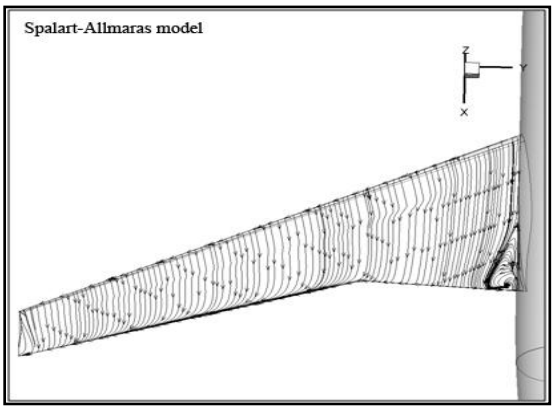

Fig 11(a). Spalart-Allmaras model

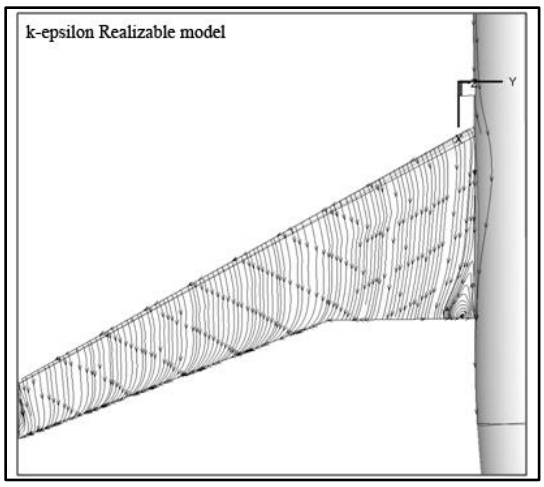

Fig 11(b).$k-\epsilon$ Realizable model

Fig 11(a-b).Streamline pattern comparison for different model at M=0.75, α=1.230

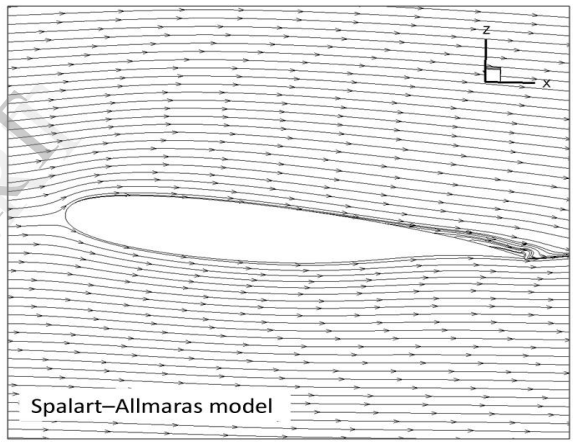

Fig 12(a).Spalart–Allmaras model

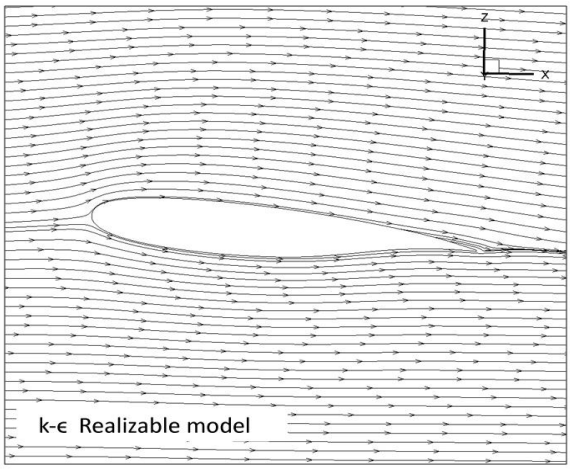

Fig 12(b).$k-\epsilon$ Realizable model

IJERT

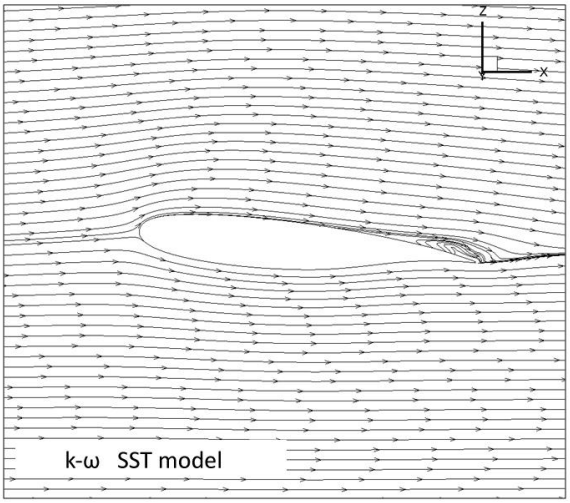

Fig 12(c).$k-\omega$ SST model

Fig 12(a-c).Streamline pattern comparison for different model at 0.150 of wing span section

7. CONCLUSION

Flow field around a wing-body configuration is investigated by carrying out Reynolds Averaged Navier-Stokes (RANS) flow simulation. Results of calculation are presented for moderate angle of attack. The steady RANS turbulence provides acceptable agreement to experimental observations. SST $k-\omega$ clearly predicts the separation region near fuselage-wing junction, when compared to realizable k-ε. It is noted that the accuracy of the computed results are dependent on a number of solver variables such as mesh configuration, numerical schemes, convergence criteria, under-relaxation factors and turbulence models employed.It is observed that for fluid problems with complex turbulent flow structures, e.g. separations, most steady-flow RANS turbulence models are able to predict the flow broadly to an agreeable extent. However, different flow regions have different best models for their flow prediction.

REFERENCES

1 John D. Anderson. Jr. (2010), "FUNDAMENTALS OF AERODYNAMICS", McGraw-Hill Book Company.
2 SatyaPrakash (2005), "Simulation of High-α Viscous Flow Around a Tactical Fighter Using RANS code CNS3D" SAROD-2005.
3 BelgharNourredine, TalbiKamel (2010), "Numerical Simulation of the Aerodynamic Characteristics of the Combined Configuration of the Wing-Body Type" European Journal of Scientific Research, ISSN 1450-216X Vol.42 No.4.
4 J. S. Mathur, K. Dhanalakshmi, V. Ramesh, S. K. Chakrabartty, (2005), "Aerodynamic Design and Analysis of SARAS Aircraft" SAROD-2005.
5 Masato Okamoto, Kunio Yasuda and Akira Azuma, 6 October (1995), "Aerodynamic Characteristics Of The Wings And Body Of A Dragonfly" The Journal of Experimental Biology 199.
6 Emily A. Leylek,Justin E. Manzo, AndEphrahim Garcia, February (2010), "Bat-Inspired Wing Aerodynamics And Optimization", Journal Of Aircraft Vol. 47, No. 1.
7 RainaldLohner, Paresh Parikh, (1988), "Generation of Three-Dimensional Unstructured Grids by the Advancing-Front Method", International Journal for Numerical Methods In Fluids, Vol. 8, 11 35-1 149
8 Alexandre P, (2011), "Numerical Simulations of Turbulent Flows Over a High-Lift Configurations", AIAA 2011-3006.

IJERT